# First-Principles Insights into Ammonia Decomposition Catalyzed by Ru Clusters Anchored on Carbon Nanotubes: Size Dependence and Interfacial Effects

Shulan Zhou,*,†,‡ Sen Lin,†,§ and Hua Guo*,†

†Department of Chemistry and Chemical Biology, University of New Mexico, Albuquerque, New Mexico 87131, United States
‡Department of Material Science and Engineering, Jingdezhen Ceramic Institute, Jingdezhen 333403, Jiangxi, China
§State Key Laboratory of Photocatalysis on Energy and Environment, College of Chemistry, Fuzhou University, Fuzhou 350002, Fujian, China
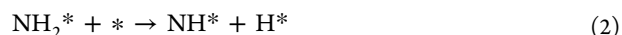
S *Supporting Information*

ABSTRACT: Ammonia decomposition catalyzed by Ru nanoparticles supported on carbon nanotubes offers an efficient way for CO_x-free hydrogen generation. To understand the catalytic mechanism, the two most important elementary steps of ammonia decomposition, namely the initial cleavage of the NH_2–H bond and the nitrogen recombination, have been studied using density functional theory on a carbon nanotube deposited with Ru_x (x = 1, 2, 6, and 13) clusters. The results indicate the reaction steps are catalyzed at Ru sites with barriers significantly lower than those on Ru(0001), but the barriers have a strong dependence on the size of the cluster. It is also found that Ru sites at the interface with the carbon nanotube are more active, showing a strong interfacial effect due apparently to facile charge transfer from the carbon nanotube to interfacial metal atoms.
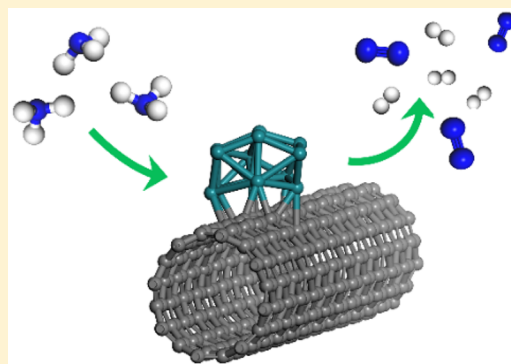
1. INTRODUCTION

Due to the well-known difficulties in storing and transporting H_2, there is currently strong interest in on-site hydrogen generation for proton exchange membrane fuel cells.[1] When carbonaceous molecules (e.g., CH_4 and CH_3OH) are used, however, CO_x (x = 1, 2) byproducts are inevitable, which can degrade the cell electrodes even at low concentrations.[2] Ammonia offers an attractive alternative for hydrogen production, serving as a CO_x-free hydrogen carrier with a high hydrogen content (17.7 wt %). As the reverse Bosch–Haber process, ammonia decomposition yields H_2 and N_2 ($NH_3 \rightarrow 3/2H_2 + 1/2N_2$, ΔH^0 = 46 kJ/mol). Importantly, ammonia decomposition has a few distinct advantages. First, ammonia can be easily liquified by either lowering temperature or increasing pressure, making it easy for storage and transportation. Second, a mature infrastructure exists for its large-scale production and distribution. Finally, ammonia is relatively stable and safe. For these reasons, on-site hydrogen generation via ammonia decomposition has attracted much recent attention.[3−6] It is important to note that the decomposition reaction is extremely slow without a catalyst. Considerable studies have thus been carried out in searching for efficient catalysts. Several transition metals, including Ru, Fe, Pt, Pd, Ir, Ni, and Rh, as well as bimetallic alloys,[7] have been tested for catalyzing the decomposition of ammonia, and these studies indicated that Ru is the most active catalyst.[3,5,6]

A better mechanistic understanding of ammonia decomposition on Ru-based catalysts will help in the design of more effective catalysts. To this end, the vast literature on ammonia synthesis[8,9] provides a useful backdrop. It is reasonably well established that the catalyzed decomposition of ammonia proceeds through the following elementary steps (* indicates an open site and X* is the adsorbed form of X):[10]

$$NH_3^* + * \rightarrow NH_2^* + H^* \tag{1}$$

$$NH_2^* + * \rightarrow NH^* + H^* \tag{2}$$

$$NH^* + * \rightarrow N^* + H^* \tag{3}$$

$$H^* + H^* \rightarrow H_2 + 2* \tag{4}$$

$$N^* + N^* \rightarrow N_2 + 2* \tag{5}$$

In ammonia synthesis, the dissociation of N_2 is well-known as the rate-limiting step.[9] In the reverse reaction, however, the situation is not as clear. Earlier experimental studies are somewhat ambiguous on the rate-determining step of ammonia decomposition on Ru surfaces. In 1987, for example, Tsai and Weinberg[11] found that the rate-determining step of NH_3 decomposition on Ru(0001) is temperature dependent. At
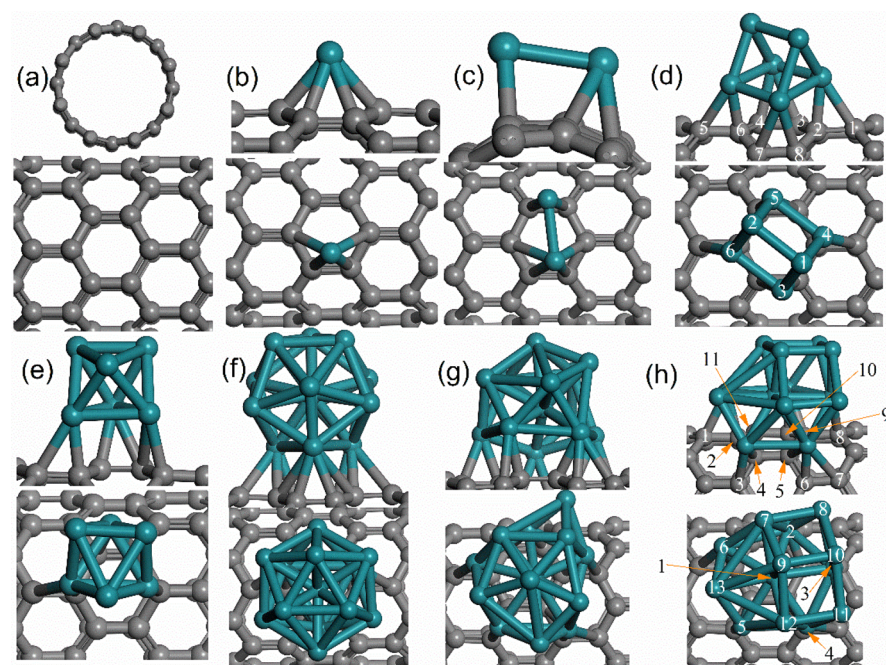
Figure 1. Side and top views of geometries of CNT (a), Ru_1@CNT (b), Ru_2@CNT (c), Ru_6@CNT (d and e), and Ru_{13}@CNT (f−h). The C and Ru atoms are colored in gray and cyan, respectively. The Ru atoms are labeled in (h).

lower temperatures, the reaction rate is determined by the recombinative desorption of nitrogen, while at temperatures above 750 K, the cleavage of the N−H bond in ammonia becomes the slowest step. However, later reports[12,13] suggested that the reaction rate is limited only by the recombinative desorption of nitrogen. Based on their studies of the kinetics of ammonia decomposition on carbon and alumina supported Ru particles, Bradford et al.[14] proposed that both the NH_2−H bond cleavage and recombinative nitrogen desorption are the slowest kinetic steps. In 2002, Chellappa et al.[15] investigated the ammonia decomposition kinetics over Ni−Pt/Al_2O_3 between temperatures of 520 and 690 °C and at ammonia pressures between 50 and 780 Torr. They concluded that the reaction rate of ammonia decomposition is limited by the recombinative desorption of nitrogen. The more recent studies on ammonia decomposition kinetics on supported Ru clusters[16] and the temperature programmed desorption of N_2 on supported Ru catalysts[17,18] also reached a similar conclusion. It appears that the rate-determining step depends on the type of catalyst and operating conditions. This kinetic complexity seems to be borne out by kinetic models.[19,20]

Theoretical understanding of ammonia decomposition on Ru catalysts has relied heavily on the vast amount of work on ammonia synthesis.[21−27] From the extensive study of ammonia synthesis on flat Ru(0001) by Nørskov and co-workers,[21,24,25] it is known the dissociation of N−N has the highest barrier. It is also the slowest step for ammonia decomposition on the same surface, with a high barrier about 2.4 eV.[24] This barrier is drastically reduced at step sites (about 1.2 eV),[24] while the barrier of some dehydrogenation step becomes higher.[24] As a result, the latter could become rate-limiting. It is interesting to note that the active sites for ammonia synthesis may be not those for ammonia decomposition.[28]

Experimental studies have also shown that the activity of the Ru catalyst is support-dependent.[2,17,29−34] Au and co-workers[3] compared the NH_3 conversion and hydrogen formation rates on Ru catalysts supported on carbon nanotubes (CNTs), MgO,

TiO_2, ZrO_2, and Al_2O_3. These investigators found that CNTs are the most effective support, and reported an activation energy of 0.72 eV for the Ru_x@CNT catalyzed ammonia decomposition.[17] It was further discovered that the catalytic activity of Ru strongly correlates with the extent of graphitization, which is attributed to the conductance of the graphitic carbon.[35,36] Moreover, the decomposition rate of NH_3 is strongly dependent on the size and shape of the Ru nanoparticles, and those with a mean size ranging from about 2 to 5 nm usually show the highest activity.[16,35,37−39] So far, however, there has been no systematic theoretical study on ammonia decomposition by supported Ru catalysts. As a result, our understanding of this important catalytic process is rather limited.

In this work, we report the first systematic theoretical study of the ammonia decomposition on Ru clusters anchored on CNTs using plane-wave density functional theory (DFT). Our work focuses on the initial cleavage of the NH_2−H bond and the recombination of N_2, namely reactions 1 and 5. The choice of these two elementary steps is motivated by the uncertainty on the rate-limiting step in this reaction. The size effect of the CNT-supported Ru cluster is investigated by examining a single Ru atom (Ru_1), the Ru dimer (Ru_2), and small Ru clusters with six (Ru_6) and 13 atoms (Ru_{13}), all supported on a CNT (denoted as Ru_x@CNT). The adsorption and reaction on different Ru sites are also studied to identify the most active sites for the catalysis. These studies help us to understand the experimental observations and to gain insights into key issues related to this important catalytic process.

2. COMPUTATIONAL DETAILS

Spin-polarized DFT as implemented in Vienna Ab initio Simulation Package (VASP)[40,41] is used in all calculations with the generalized gradient approximation (GGA) functional of Perdew, Burke, and Ernzerhof (PBE).[42] The valence electronic wave functions are expanded in plane waves with an energy

cutoff of 400 eV, and the projector-augmented wave (PAW) approach[43] was employed for the core electrons. The supercell model was built based on the (8,0) zigzag single-wall CNT. For the Ru_1 and Ru_2 clusters, a $20 \times 20 \times 8.52$ Å³ supercell was used, while for the larger Ru_6 and Ru_{13} clusters, a $20 \times 20 \times 12.78$ Å³ supercell was used to avoid interaction among neighboring images. For these two types of supercells, $1 \times 1 \times 4$ and $1 \times 1 \times 3$ Monkhorst–Pack k-points[44] were selected to sample the Brillouin zone. For the calculation of the density of states (DOS), a $1 \times 1 \times 11$ Monkhorst–Pack k-point grid was employed. Van der Waals corrections were included using the DFT-D2 method of Grimme.[45]

The binding energy of Ru_x cluster on the CNT was calculated using the equation $E_b = E(Ru_x@CNT) - E(CNT) - E(Ru_x)$, and the adsorption energy of a pertinent species (X) is obtained via the equation $E_{ad} = E(X-Ru_x@CNT) - E(Ru_x@CNT) - E(X)$. The transition states (TSs) between stable initial states (ISs) and final states (FSs) were determined using the climb image nudged elastic band (CI-NEB) method.[46] Atomic charges were computed using the atom-in-molecule (AIM) scheme proposed by Bader.[47] The charge density differences were evaluated using the formula $\Delta\rho = \rho_{A+B} - \rho_A - \rho_B$, where ρ_M is the electron density of M. The convergence of relaxation was checked with the 0.05 eV/Å criterion, and the total energy difference is less than 1×10^{-4} eV.

3. RESULTS

3.1. Structure and Stability of $Ru_x@CNT$ ($x = 1, 2, 6,$ and 13). The optimized geometries of the CNT and $Ru_x@CNT$ ($x = 1, 2, 6,$ and 13) are shown in Figure 1. There are two types of C−C bonds in the CNT with lengths about 1.42 and 1.44 Å, which are very similar to the previous results of Verdinelli et al.[48] When Ru_x is anchored on the CNT, the C−C bond lengths close to the metal atoms change only slightly. For $Ru_1@CNT$, the Ru atom is located on a hollow site with four Ru−C bond lengths of 2.12, 2.12, 2.27, and 2.27 Å, respectively. The corresponding binding energy is −2.255 eV, which is again in good agreement with the earlier result of Verdinelli et al.[48] For $Ru_2@CNT$, one Ru atom is located at a hollow site and the other is located at a neighboring bridge site. The Ru−Ru distance is 2.32 Å, which is slightly longer than that of the free Ru dimer (2.20 Å). The corresponding binding energy of Ru_2 on the CNT is −2.022 eV, which is slightly lower than that of $Ru_1@CNT$ (−2.255 eV).

For the isolated Ru_6 cluster, two stable geometries were found, as shown in Figure 2a,b. The geometry in Figure 2a is about 0.52 eV more stable than that in Figure 2b, which is consistent with the earlier result of Wang and Johnson.[49] Geometries of the two clusters anchored on the CNT are both three-dimensional, as shown in Figure 1d,e. For Figure 1d ($E_b =$
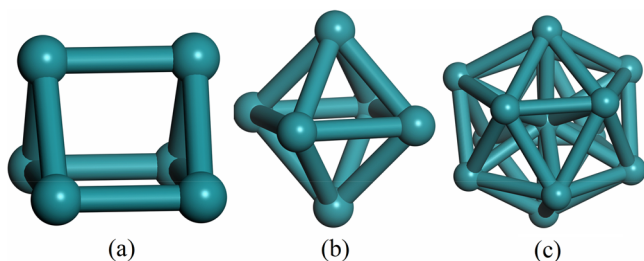
−4.673 eV), four Ru atoms are bonded to CNT and two are on top, forming the interfacial and top layers. For Figure 1e ($E_b =$ −3.645 eV), only three Ru atoms are in contact with the CNT wall and three are on the top layer. Since the binding of the former is about 1 eV stronger than the latter on the CNT, the more stable geometry of Figure 1d is selected to study the ammonia decomposition below.

For the isolated Ru_{13} cluster, there are numerous possible minima. The search of the global minimum requires highly sophisticated methods such as molecular dynamics or genetic algorithms. In addition, the most stable geometry may depend on the DFT method used in the calculation.[50−52] Moreover, the fluxional nature of the metal cluster and the easy interconversion between different isomers may further complicate the situation.[53] On a support, the structure and energetics of such a cluster are even more complex. Therefore, in this work we selected the Ru_{13} cluster with the icosahedral symmetry as the starting structure, which was previously used by Liu et al.[54] and by Gao and Zhao,[55] in their studies of Ru nanoparticles supported on graphene and CNT, respectively. The optimized geometry of the freestanding Ru_{13} cluster is given in Figure 2c, in which the calculated Ru−Ru distance ranges from 2.48 to 2.70 Å, in good agreement with the results of Liu et al.[54] On the CNT, several optimized geometries were obtained starting from this icosahedral structure. Three selected optimized geometries of $Ru_{13}@CNT$ are shown in Figure 1f−h. Figure 1f ($E_b = -4.604$ eV) still retains some original icosahedral structure, while geometries in Figure 1g,h are distorted, presumably due to strong interaction with the CNT. All these structures are three-dimensional with multiple layers of Ru atoms. The binding of Figure 1h ($E_b = -6.975$ eV) is about 2.38 and 1.08 eV more stable than Figure 1, geometries f and g ($E_b = -5.902$ eV), respectively. This work thus focus on Figure 1h for the possible reactive sites and support effects on ammonia decomposition.

3.2. Adsorption of Pertinent Species. The adsorption geometries of pertinent species on the bare CNT are shown in Figure 3, and the corresponding adsorption energies are listed in Table 1. The adsorption of these species has a minor influence on the geometry of CNT. For NH_3, it adsorbs with the nitrogen end with a N−CNT distance of 3.18 Å. The adsorption energy is −0.107 eV, suggesting a very weak physical adsorption. Both NH_2 and H adsorbed strongly atop C, however, the former with its nitrogen end. The calculated adsorption energy of H is −1.562 eV, which is in excellent agreement with the result (−1.595 eV) of Verdinelli et al.[48] The adsorption energy for NH_2 is comparable (−1.136 eV).

The adsorption geometries of pertinent species on $Ru_x@CNT$ ($x = 1, 2$) are given in Figure 3, and the adsorption energies are shown in Table 1. On $Ru_1@CNT$, NH_3 and NH_2 are adsorbed on Ru with adsorption energies of −1.426 and −3.537 eV, respectively, which are stronger than those on Ru(0001).[23] For H, it is also bonded to a Ru atom with a Ru−H bond length of 1.59 Å and an adsorption energy of −2.935 eV, similar to that on Ru(0001).[23] In this geometry, due to the effect of support, H is tilted toward CNT.[48] On $Ru_2@CNT$, the adsorption energy of NH_3 is very close to that on $Ru_1@CNT$. For NH_2 and H, the adsorption of these species on $Ru_2@CNT$ is slightly stronger than on $Ru_1@CNT$. But for the products, NH_2 and H are adsorbed on two different Ru atoms, while on $Ru_1@CNT$ they have to share the same Ru atom.

On $Ru_2@CNT$, N adsorbs chemically on top of Ru with a tilt. The adsorption energy is −5.949 eV, which is somewhat
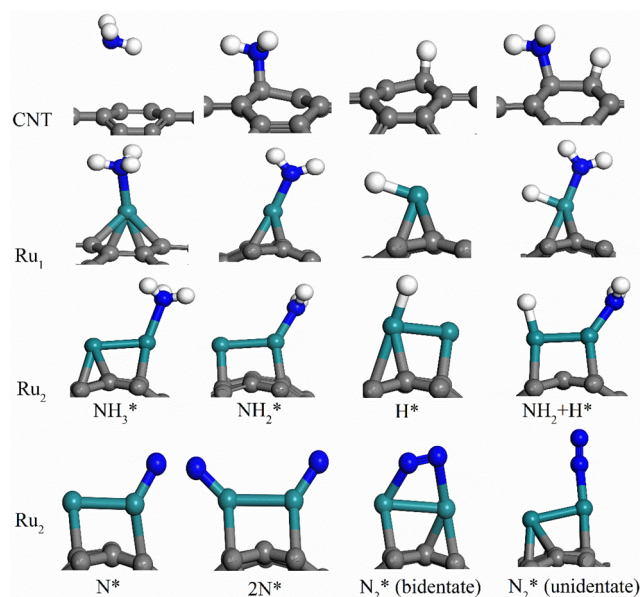

Figure 2. Geometries of isolated Ru_6 (a and b) and Ru_{13} (c).

Figure 3. Adsorption geometries of pertinent species on CNT, Ru$_1$@CNT, and Ru$_2$@CNT. The C, Ru, N, and H atoms are colored in gray, cyan, blue, and white, respectively.

Figure 4. Adsorption geometries of pertinent species on interface layer of Ru$_6$@CNT. The same color scheme as Figure 3 is used.

stronger than on Ru(0001) ($\sim$5.7–5.8 eV).[23,56] The adsorption of the second N atom is also strong. The averaged adsorption energy is 0.39 eV weaker than the first N atom, suggesting a repulsive interaction between the two N atoms in the adsorbed state. For N$_2$ adsorption, two stable adsorption geometries are obtained (see Figure 3), both with moderately strong adsorption. The first is a bidentate configuration, while the second one is unidentate on top of a Ru atom. The latter is 0.16 eV more stable than the former. Similar structures were observed on Ru(0001), but with much smaller adsorption energies.[57,58]

For Ru$_6$@CNT, there are two different kinds of active sites: interfacial and top layer sites. Because the catalytic activity may be different, both types of sites were investigated. The adsorption geometries of the pertinent species on the interface of Ru$_6$@CNT are shown in Figure 4. On both the interfacial and top layers (for top layers, see Figure S1 in the Supporting Information) sites, NH$_3$, NH$_2$, and H are all bonded to a Ru atom. It is interesting to note that the adsorption of these species on the interfacial sites are in general stronger than on
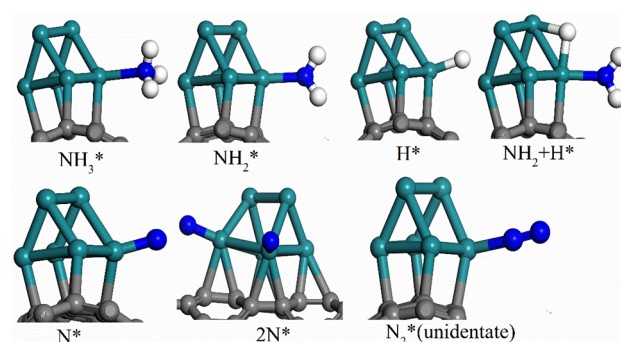
the top layer sites (see Table 1). Especially for H, the adsorption energy at an interface site is 1.278 eV larger than that on a top layer site, showing a strong interfacial effect. For atomic and molecular nitrogen, a similar pattern emerges, as shown in Table 1, although the distinction between the two types of sites is less pronounced. At the interfacial sites, N adsorbs on a top site of Ru with an adsorption energy of −5.122 eV. For 2N*, both nitrogen atoms adsorb on Ru with a N−N distance of 4.64 Å, slightly shorter than that of Ru$_2$@CNT. Different from Ru$_2$@CNT, however, N$_2$ can only adsorb on the top of Ru with unidentate N bonding to a Ru atom (see Figure 4) and its adsorption energy of −1.140 eV is about 0.47 eV larger than that on Ru(0001).[59]

Since the reaction properties discussed below also indicated that the interfacial sites are more active, only the interfacial adsorption sites are considered for Ru$_{13}$@CNT. The adsorption geometries are displayed in Figure 5. Similar to that on Ru$_x$@CNT (x = 1, 2, and 6), in the interface layer of Ru$_{13}$@CNT, NH$_3$ adsorbs at a top Ru site, consistent with the previous studies on Ru(0001).[22−24] The adsorption energy of NH$_3$ is −1.207 eV, which is smaller than those on Ru$_x$@CNT (x = 1, 2, and 6). For NH$_2$, it adsorbed on an interfacial bridge site with an adsorption energy of −3.822 eV, which is stronger than those on Ru$_x$@CNT (x = 1, 2, and 6). For H, it also prefers to adsorb on a bridge site on the interface. The adsorption energy is −2.914 eV, which is close to that on Ru$_1$@CNT and smaller than those on Ru$_2$@CNT and at the interface of Ru$_6$@CNT. The adsorption energy of a single N atom on top of an interface Ru atom is −4.883 eV. For 2N*, both N atoms are located at the top of Ru, with a coadsorption energy of −5.078 eV. The

Table 1. Calculated Adsorption Energies, Reaction Energies, and Activation Energies (all in eV) of the NH$_3$* + * → NH$_2$* + H* and 2N* → N$_2$* + * Steps in Ammonia Decomposition[a]

	CNT	Ru$_1$@CNT	Ru$_2$@CNT	Ru$_6$@CNT(interfacial)	Ru$_6$@CNT(top)	Ru$_{13}$@CNT	Ru(0001)
NH$_3$	−0.107	−1.429	−1.468	−1.409	−1.266	−1.207	−0.89[b]
NH$_2$	−1.136	−3.537	−3.659	−3.471	−3.345	−3.822	−2.95[b]
H	−1.562	−2.935	−3.189	−3.939	−2.661	−2.914	−2.98[b]
E_{r1}	0.571	−0.466	−0.232	0.140	0.176	0.455	−0.07[b]
E_{a1}	2.107	1.066	0.830	1.231	1.439	0.737	1.27[b]
N*			−5.949	−5.122	−4.853	−4.883	−5.70[b]
2N*			−5.555	−4.741	−4.866	−5.072	–
N$_2$*(bidentate)			−1.223	–		−0.586	–
N$_2$*(unidentate)			−1.380	−1.140	−0.926	−0.898	−0.67[c]
E_{r5}			−0.515	−2.028	−1.584	−0.819	–
E_{a5}			1.507	1.324		0.846	2.4[d]

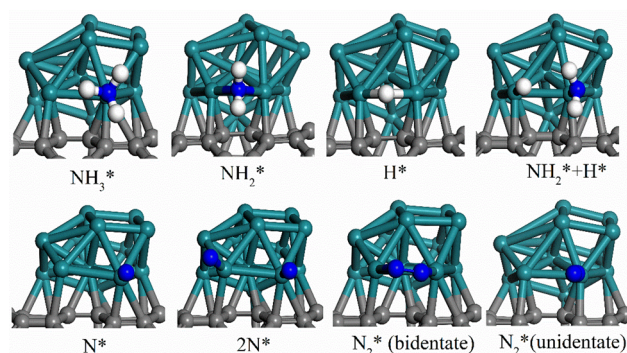[a]The DFT results on Ru(0001) are also listed for comparison. [b]Reference 23. [c]Reference 59. [d]Reference 24.

Figure 5. Adsorption geometries of pertinent species on interfacial sites of Ru$_{13}$@CNT. The same color scheme of Figure 3 is used.

N−N distance is 3.77 Å, which is about 1 Å shorter than those on Ru$_2$@CNT and Ru$_6$@CNT. For N$_2$, the bidentate form is about 0.31 eV less stable than the unidentate form.

3.3. Reactions. We will focus our studies of reaction barriers on two potential candidates of the rate-limiting step in ammonia decomposition, namely the dehydrogenation of ammonia (reaction 1) and recombination of N$_2$ (reaction 5). The desorption of N$_2$ is not considered.

The calculated reaction paths of reaction 1 on the CNT and Ru$_x$@CNT (x = 1, 2, 6, and 13) and the corresponding transition-state geometries are shown in Figure 6. The geometric parameters of these structures can be found in the Supporting Information. The reaction energy (E_r) and activation energy (E_a) are listed in Table 1. On the bare CNT, the reaction is endothermic by 0.557 eV. The calculated barrier is very high (2.107 eV), suggesting that the decomposition of ammonia on pure CNT is very difficult. This is consistent with a previous study.[60] On Ru$_1$@CNT, the reaction proceeds with an exothermicity of −0.466 eV. The barrier of 1.066 eV is about 0.20 eV lower than the corresponding value of 1.27 eV on Ru(0001)[23] and comparable with the value (about 1 eV) on stepped Ru(0001).[24] However,

the products have to share the same Ru atom, which makes further reactions impossible. On Ru$_2$@CNT, the barrier for reaction 1 is even lower (0.830 eV), suggesting a more facile reaction than on Ru$_1$@CNT or on Ru(0001). On Ru$_6$@CNT, as shown in Figure 6, it is interesting to note that the barrier for reaction 1 at interfacial sites (1.231 eV) is much lower than that at top layer sites (1.439 eV). On Ru$_{13}$@CNT, the reaction at the interfacial site of Ru$_{13}$@CNT proceeds with a barrier of about 0.737 eV with an endothermicity of 0.455 eV. The barrier is significantly lower than that on Ru$_6$@CNT and even lower than that on Ru$_2$@CNT.

The reaction paths of N$_2$* formation (reaction 5) on Ru$_x$@CNT (x = 2, 6, and 13) are presented in Figure 7, with the transition-state geometries. The reaction and activation energies are listed in Table 1. The internuclear distances for these structures are also provided in the Supporting Information. The barrier of the formation of N$_2$* on Ru$_2$@CNT is 1.507 eV, which is about 0.91 eV lower than that on Ru(0001),[24] but is about 0.31 eV higher than the value of 1.2 eV on stepped Ru(0001).[24] On Ru$_6$@CNT, the barrier of reaction 5 is 1.324 eV, which is 0.18 eV lower than on Ru$_2$@CNT and about 0.12 eV higher than that on the stepped Ru(0001).[24] On Ru$_{13}$@CNT, the barrier is significantly reduced to 0.846 eV, which is more than 1.5 eV lower than on Ru(0001) and is about 0.66 and 0.48 eV lower than on Ru$_2$@CNT and Ru$_1$@CNT, respectively. In addition, the barrier is very close to the experimental apparent activation energy of ammonia decomposition.[17]

4. DISCUSSION

Overall, the adsorption of the pertinent species on Ru$_x$@CNT is much stronger than that on the CNT, and the corresponding reaction barriers are much lower, too. These results practically rule out the CNT as the catalyst. Comparing with Ru(0001), the barriers for both reactions 1 and 5 are consistently lower. This is particularly true for reaction 5, which is the rate-limiting step on Ru(0001), as the barrier height is reduced by more than
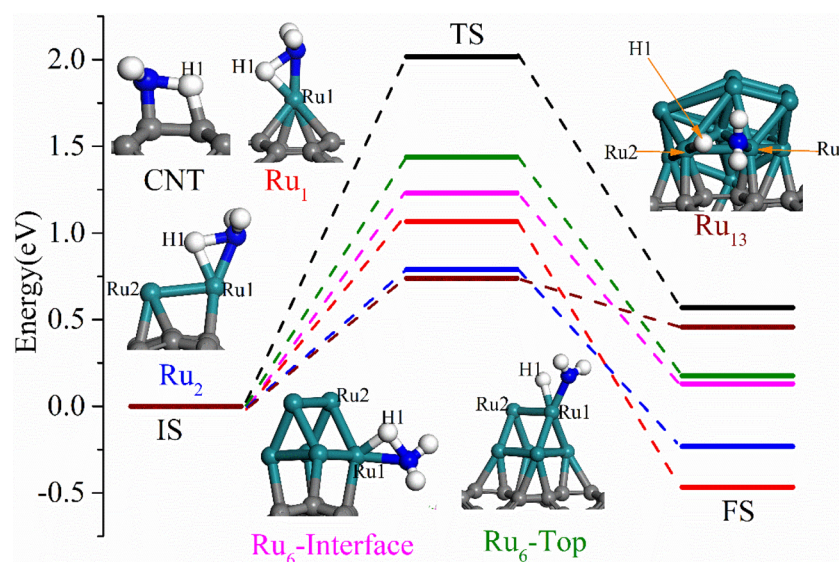

Figure 6. Reaction paths of NH$_3$* → NH$_2$* + H* on CNT (black line), Ru$_1$@CNT (red line), Ru$_2$@CNT (blue line), interfacial sites of Ru$_6$@CNT (magenta line), top layer sites of Ru$_6$@CNT (olive line), and Ru$_{13}$@CNT (wine line). The geometries of transition states (TSs) are also given. The geometries of initial state (IS) and final state (FS) are referred to the corresponding geometries of NH$_3$ and NH$_2$ + H shown in Figures 3−5. The same color scheme as Figure 3 is used.
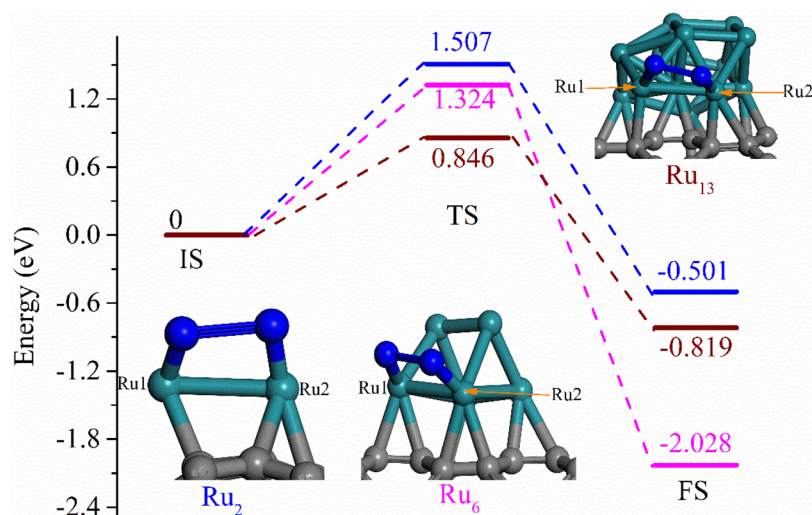
Figure 7. Calculated reaction paths of N_2 formation on Ru$_2$@CNT (blue line), Ru$_6$@CNT (magenta line), and Ru$_{13}$@CNT (wine line). The geometries of transition states are also given. The geometries of initial state (IS) and final state (FS) are referred to the corresponding geometries of 2N* and N_2* shown in Figures 3−5. The same color scheme as Figure 3 is used.

1 eV. The significantly lowered barriers on Ru$_x$@CNT are consistent with the presence of uncoordinated sites in the supported Ru clusters.

Due to limitations in computing power, however, it is still impossible to investigate the ammonia decomposition on experimentally relevant Ru nanoparticles (2−5 nm in size) anchored on CNTs. Nevertheless, the results presented in this work provide useful information on several important issues in this catalytic process, such as size effects and active sites.

In Figure 8, activation energies for both reactions 1 and 5 are plotted as a function of the Ru cluster size (x). The results on
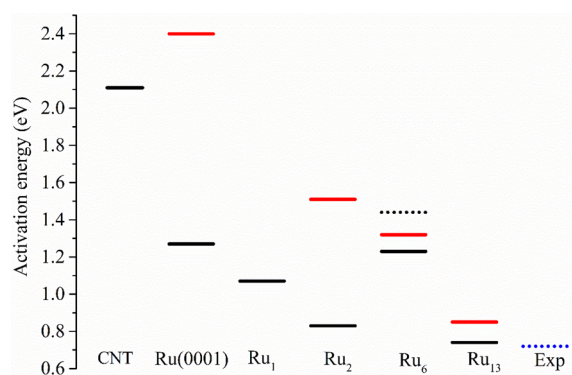

Figure 8. Size dependence of activation energy for ammonia dehydrogenation (reaction 1) and nitrogen recombination (reaction 5). Solid black line, reaction 1; solid red line, reaction 5. Here Ru$_x$ (x = 1, 2, 6, and 13) indicates the corresponding Ru$_x$@CNT. For Ru$_6$@CNT, the solid lines give the results on the interface while the black dotted line displays the results of reaction 1 on top layer sites. The DFT results on Ru(0001) are also given, while the blue dotted line indicates the experimental apparent activation energy.

Ru(0001) and the experimentally measured apparent activation energy are also included for comparison. It is clear from Figure 8 that the recombination of nitrogen (reaction 5) has consistently higher barriers than the dehydrogenation of ammonia (reaction 1). This trend is the same as with previous theoretical studies on the (0001) facet of Ru,[24,25] as well as most kinetic studies.[16,17,34] However, it is also clear that there is

no clear trend in the size effect, as the barriers do not change monotonically with the number of Ru atoms in the supported cluster. This is not inconsistent with experimental observations of strong size effects.[15,34,36−38] The experimentally observed optimal size of 2−5 nm contains hundreds of Ru atoms, which are unfortunately beyond our current ability.

The calculations reported here also suggest strong interfacial effects. In particular, the Ru sites near the CNT surface exhibit stronger adsorption and lower reaction barriers. Similar interfacial effects have previously been noted in DFT studies of reactions catalyzed by nanoclusters supported on oxide surfaces by several researchers.[61−65] In these studies, the catalysis at the interfacial sites was found either to have lower barriers or to proceed via different reaction paths.

An important characteristic of the interfacial effect is the amount of charge transfer at the interface. To understand this effect, we computed the Bader charges of Ru atoms in Ru$_{13}$@CNT and Ru$_6$@CNT, and the results are listed in Table 2 and Table S3, respectively. In addition, the differential charge densities of Ru$_{13}$@CNT and Ru$_6$@CNT are shown shown in Figure 9 and Figure S2 with two isovalues, respectively. In Figure 9a, it is clear that the Ru atoms in the interfacial layer have much more positive charges than those in the upper layer. This suggests that the charge transfer from CNT is much more facile in the interfacial layer, and as a result the Ru atoms in this layer are much more oxidic. This explains the stronger adsorption and lower reaction barriers at the interfacial sites observed in our DFT calculations. It is interesting to note the observed correlation between the catalytic activity of ammonia decomposition and the extent of graphenization of the carbon support.[35,36] It is possible that the better conductivity of the CNT, that allows more facile charge transfer to the interfacial layer, is responsible for the enhanced activity of these catalysts. Indeed, in Figure 9b, it is clear that the charge depletion is not restricted to the carbon atoms at the interface with Ru, but spreads out to the entire CNT. This nonlocal charge transfer presumably stems from the conducted characteristic of the CNT.

The strong interaction between the interfacial Ru atoms and carbon atoms in the CNT is also supported by the projected density of states (PDOS), as shown in Figure 10 and Figure S3.

Table 2. Calculated Bader Charges ($|e|$) for Carbon and Ruthenium Atoms in the Ru$_{13}$@CNT System As Shown in Figure 1[a]

	atom	Bader charge
interfacial layer	Ru$_1$	0.30
	Ru$_2$	0.19
	Ru$_3$	0.22
	Ru$_4$	0.20
	Ru$_5$	0.19
	Ru$_6$	0.17
$Q_{interface\_Ru}$		1.27
upper layer	Ru$_7$	−0.05
	Ru$_8$	−0.05
	Ru$_9$	0.04
	Ru$_{10}$	−0.02
	Ru$_{11}$	−0.04
	Ru$_{12}$	−0.04
	Ru$_{13}$	−0.04
Q_{upper_Ru}		−0.20
Q_{all_Ru}		1.07
interfacial layer	C$_1$	−0.09
	C$_2$	−0.07
	C$_3$	−0.06
	C$_4$	−0.11
	C$_5$	−0.07
	C$_6$	−0.11
	C$_7$	−0.09
	C$_8$	−0.07
	C$_9$	−0.13
	C$_{10}$	−0.07
	C$_{11}$	−0.09
$Q_{interface\_C}$		−0.96
Q_{all_C}		−1.07

[a]The sum of all (interfacial) C charges is given by Q_{all_C} ($Q_{interface\_C}$), while the sum of all (interfacial) Ru charges is given by Q_{all_Ru} ($Q_{interface\_Ru}$). The atomic labels are defined in Figure 1.

The Ru$_{13}$ and Ru$_6$ clusters without the CNT exhibit d bands consisting of sharp features ranging from −6 to 4 eV, while after binding with the CNT the d bands become broader with a range from −8 to 6.5 eV. We can also see strong coupling between the Ru d orbitals and the 2p orbitals of the interfacial carbon atoms, suggesting covalent bonding. The broadened and significantly modified DOS of Ru reveals a strong hybridization of the Ru cluster with the CNT support, underscoring the significant redistribution of charge at the interface between Ru and CNT.

In addition, geometric effects also play a role in the variation of the activities. For Ru$_6$@CNT, the reactions occur on the sides of a square formed by four Ru atoms, while for Ru$_{13}$@CNT, the reactions take place on the sides of a triangle formed by three Ru atoms. For the former, one Ru atom is responsible for the breaking of the NH$_2$−H bond, while for the latter, two Ru atoms contribute to the cleavage of the NH$_2$−H bond. Moreover, the adsorption geometry of N$_2$ also suggests an influence of geometry. On Ru$_6$@CNT, only the unidentate adsorption geometry of N$_2$ is stable, while on Ru$_{13}$@CNT, two stable adsorption geometries were found.

5. CONCLUSIONS

In this work, the initial cleavage of NH$_2$−H bond and the nitrogen recombination related to ammonia decomposition are studied systematically using DFT on Ru$_x$@CNT (x = 1, 2, 6, and 13). Our results indicate that the nitrogen recombination is the rate-limiting step throughout, although the barrier heights depend sensitively on the size of the Ru clusters. These results also suggest that Ru clusters on the CNT significantly lower the barriers of these two elementary processes relative to the Ru(0001) surface, due apparently to the presence of uncoordinated sites in the cluster. The barrier lowering is particularly pronounced for the rate-limiting nitrogen recombination step. Comparing with experiment, the calculated activation energy for Ru$_{13}$@CNT is quite close to the apparent activation energy measured on Ru clusters supported by CNTs. Furthermore, it was found that the reactions have lower barriers at the Ru sites at the Ru−CNT interface, due apparently to the facile charge transfer from the CNT to the Ru atoms. These insights shed valuable light on the mechanism of ammonia decomposition catalyzed by Ru clusters supported on CNTs. However, it is still premature to compare the theoretical results to actual catalysts because the sizes of the Ru clusters in this
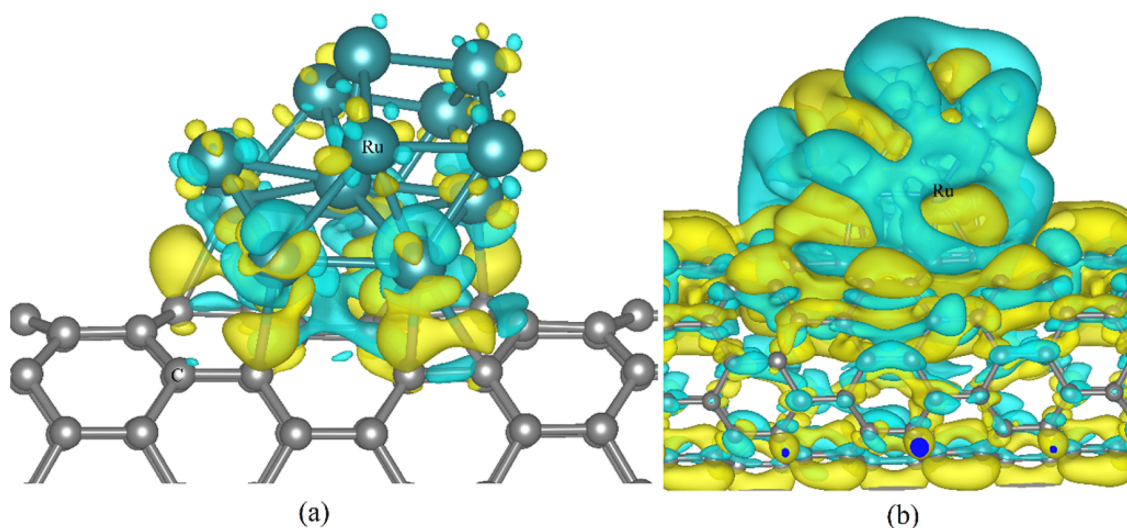

Figure 9. Contour plots of differential charge density of Ru$_{13}$@CNT. The charge accumulation region is rendered in yellow, while the charge depletion region is in blue. The isosurface level is ±0.005 and ±0.00008 au for (a) and (b), respectively. Color code: C, gray; Ru, cyan.
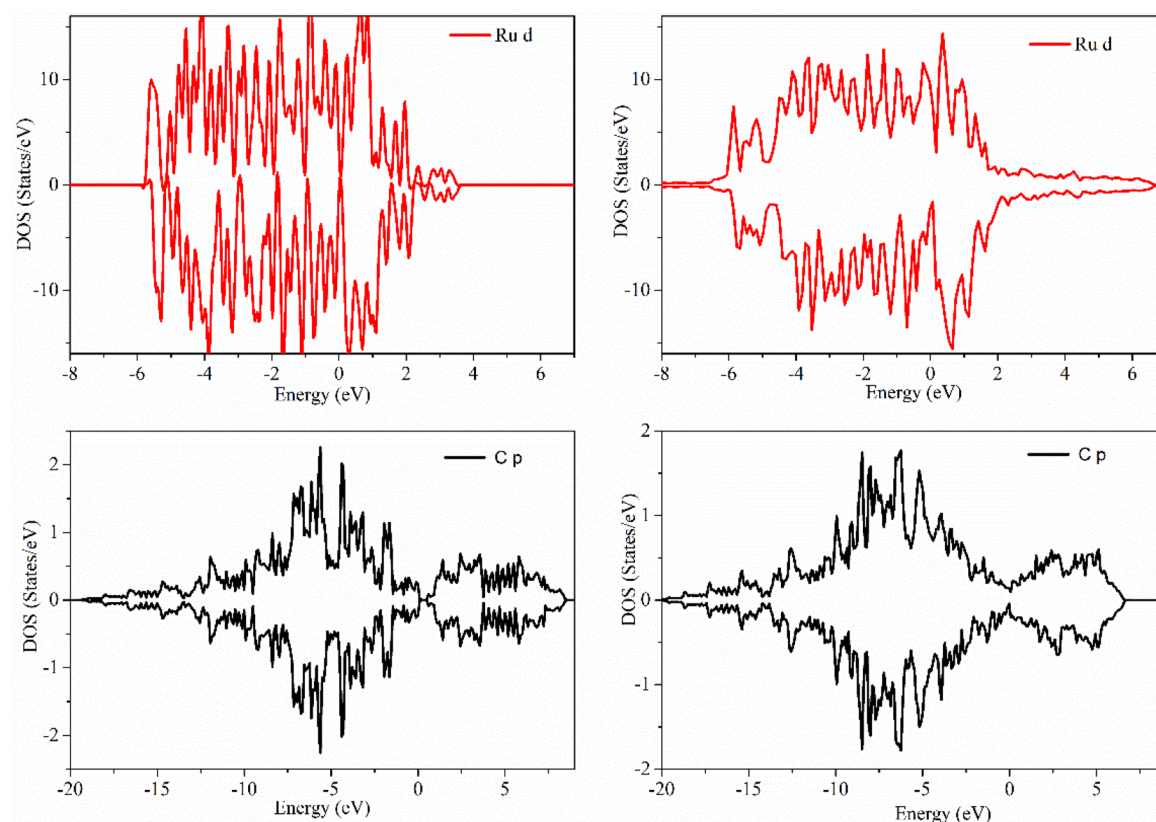
Figure 10. Projected densities of states (PDOSs) of d orbitals of Ru_{13} (upper panels) and p orbitals of interfacial carbons in CNT (lower panels). The left column is for individual Ru_{13} and CNT, while the right column is for the combined system. The Fermi level is set to 0 eV.

work are still too small. More studies are needed to explore the catalysis with Ru nanoparticles with 2−5 nm sizes to ascertain the effects observed in this work.

ASSOCIATED CONTENT

Ⓢ Supporting Information

The Supporting Information is available free of charge on the ACS Publications website at DOI: 10.1021/acs.jpcc.8b01965.

> Additional results on adsorbate geometries, charges of atoms in the clusters, differential charge densities, densities of states, and transition state geometries (PDF)

AUTHOR INFORMATION

Corresponding Authors
*E-mail: zhoushulan2009@126.com.
*E-mail: hguo@unm.edu.

ORCID Ⓘ

Sen Lin: 0000-0002-2288-5415
Hua Guo: 0000-0001-9901-053X

Notes

The authors declare no competing financial interest.

REFERENCES

(1) Schlapbach, L.; Züttel, A. Hydrogen-storage materials for mobile applications. *Nature* **2001**, *414*, 353−358.

(2) Choudhary, T. V.; Sivadinarayana, C.; Goodman, D. W. Catalytic ammonia decomposition: CO_x-free hydrogen production for fuel cell applications. *Catal. Lett.* **2001**, *72*, 197−201.

(3) Yin, S. F.; Xu, B. Q.; Zhou, X. P.; Au, C. T. A mini-review on ammonia decomposition catalysts for on-site generation of hydrogen for fuel cell applications. *Appl. Catal., A* **2004**, *277*, 1−9.

(4) Christensen, C. H.; Johannessen, T.; Sørensen, R. Z.; Nørskov, J. K. Towards an ammonia-mediated hydrogen economy? *Catal. Today* **2006**, *111*, 140−144.

(5) Klerke, A.; Christensen, C. H.; Norskov, J. K.; Vegge, T. Ammonia for hydrogen storage: challenges and opportunities. *J. Mater. Chem.* **2008**, *18*, 2304−2310.

(6) Schüth, F.; Palkovits, R.; Schlogl, R.; Su, D. S. Ammonia as a possible element in an energy infrastructure: catalysts for ammonia decomposition. *Energy Environ. Sci.* **2012**, *5*, 6278−6289.

(7) Hansgen, D. A.; Vlachos, D. G.; Chen, J. G. Using first principles to predict bimetallic catalysts for the ammonia decomposition reaction. *Nat. Chem.* **2010**, *2*, 484−489.

(8) Ertl, G. Primary steps in catalytic synthesis of ammonia. *J. Vac. Sci. Technol., A* **1983**, *1*, 1247−1253.

(9) Hellman, A.; Baerends, E. J.; Biczysko, M.; Bligaard, T.; Christensen, C. H.; Clary, D. C.; Dahl, S.; van Harrevelt, R.; Honkala, K.; Jonsson, H.; et al. Predicting catalysis: Understanding

ammonia synthesis from first-principles calculations. *J. Phys. Chem. B* **2006**, *110*, 17719−17735.

(10) Hellman, A.; Honkala, K.; Remediakis, I. N.; Logadóttir, Á.; Carlsson, A.; Dahl, S.; Christensen, C. H.; Nørskov, J. K. Ammonia synthesis and decomposition on a Ru-based catalyst modeled by first-principles. *Surf. Sci.* **2009**, *603*, 1731−1739.

(11) Tsai, W.; Weinberg, W. H. Steady-state decomposition of ammonia on the ruthenium(001) surface. *J. Phys. Chem.* **1987**, *91*, 5302−5307.

(12) Egawa, C.; Nishida, T.; Naito, S.; Tamaru, K. Ammonia decomposition on (1110) and (001) surfaces of ruthenium. *J. Chem. Soc., Faraday Trans. 1* **1984**, *80*, 1595−1604.

(13) Vitvitskii, A.; Gaidei, T.; Toporkova, M.; Kiseleva, E.; Melikhov, E. Kinetics of catalytic decomposition of ammonia. *J. Appl. Chem. USSR* **1990**, *63*, 1883−1886.

(14) Bradford, M. C. J.; Fanning, P. E.; Vannice, M. A. Kinetics of NH_3 decomposition over well dispersed Ru. *J. Catal.* **1997**, *172*, 479−484.

(15) Chellappa, A. S.; Fischer, C. M.; Thomson, W. J. Ammonia decomposition kinetics over Ni-Pt/Al_2O_3 for PEM fuel cell applications. *Appl. Catal., A* **2002**, *227*, 231−240.

(16) Zheng, W.; Zhang, J.; Xu, H.; Li, W. NH_3 decomposition kinetics on supported Ru clusters: Morphology and particle size effect. *Catal. Lett.* **2007**, *119*, 311−318.

(17) Yin, S.-F.; Zhang, Q.-H.; Xu, B.-Q.; Zhu, W.-X.; Ng, C.-F.; Au, C.-T. Investigation on the catalysis of CO_x-free hydrogen generation from ammonia. *J. Catal.* **2004**, *224*, 384−396.

(18) Hayashi, F.; Toda, Y.; Kanie, Y.; Kitano, M.; Inoue, Y.; Yokoyama, T.; Hara, M.; Hosono, H. Ammonia decomposition by ruthenium nanoparticles loaded on inorganic electride C12A7:e. *Chemical Science* **2013**, *4*, 3124−3130.

(19) Prasad, V.; Karim, A. M.; Arya, A.; Vlachos, D. G. Assessment of overall rate expressions and multiscale, microkinetic model uniqueness via experimental data injection: Ammonia decomposition on Ru/γ-Al_2O_3 for hydrogen production. *Ind. Eng. Chem. Res.* **2009**, *48*, 5255−5265.

(20) Ulissi, Z.; Prasad, V.; Vlachos, D. G. Effect of multiscale model uncertainty on identification of optimal catalyst properties. *J. Catal.* **2011**, *281*, 339−344.

(21) Dahl, S.; Logadottir, A.; Egeberg, R. C.; Larsen, J. H.; Chorkendorff, I.; Tornqvist, E.; Nørskov, J. K. Role of steps in N_2 activation on Ru(0001). *Phys. Rev. Lett.* **1999**, *83*, 1814−1817.

(22) Zhang, C.; Liu, Z.-P.; Hu, P. Stepwise addition reactions in ammonia synthesis: A first principles study. *J. Chem. Phys.* **2001**, *115*, 609−611.

(23) Zhang, C. J.; Lynch, M.; Hu, P. A density functional theory study of stepwise addition reactions in ammonia synthesis on Ru(0 0 0 1). *Surf. Sci.* **2002**, *496*, 221−230.

(24) Logadóttir, Á.; Nørskov, J. K. Ammonia synthesis over a Ru(0001) surface studied by density functional calculations. *J. Catal.* **2003**, *220*, 273−279.

(25) Honkala, K.; Hellman, A.; Remediakis, I. N.; Logadottir, A.; Carlsson, A.; Dahl, S.; Christensen, C. H.; Nørskov, J. K. Ammonia synthesis from first-principles calculations. *Science* **2005**, *307*, 555−558.

(26) Howalt, J. G.; Bligaard, T.; Rossmeisl, J.; Vegge, T. DFT based study of transition metal nano-clusters for electrochemical NH_3 production. *Phys. Chem. Chem. Phys.* **2013**, *15*, 7785−7795.

(27) Ishikawa, A.; Doi, T.; Nakai, H. Catalytic performance of Ru, Os, and Rh nanoparticles for ammonia synthesis: A density functional theory analysis. *J. Catal.* **2018**, *357*, 213−222.

(28) Boisen, A.; Dahl, S.; Nørskov, J. K.; Christensen, C. H. Why the optimal ammonia synthesis catalyst is not the optimal ammonia decomposition catalyst. *J. Catal.* **2005**, *230*, 309−312.

(29) Raróg-Pilecka, W.; Szmigiel, D.; Kowalczyk, Z.; Jodzis, S.; Zielinski, J. Ammonia decomposition over the carbon-based ruthenium catalyst promoted with barium or cesium. *J. Catal.* **2003**, *218*, 465−469.

(30) Wang, S. J.; Yin, S. F.; Li, L.; Xu, B. Q.; Ng, C. F.; Au, C. T. Investigation on modification of Ru/CNTs catalyst for the generation of COx-free hydrogen from ammonia. *Appl. Catal., B* **2004**, *52*, 287−299.

(31) Yin, S. F.; Xu, B. Q.; Zhu, W. X.; Ng, C. F.; Zhou, X. P.; Au, C. T. Carbon nanotubes-supported Ru catalyst for the generation of COx-free hydrogen from ammonia. *Catal. Today* **2004**, *93−95*, 27−38.

(32) Yin, S.-F.; Xu, B.-Q.; Ng, C.-F.; Au, C.-T. Nano Ru/CNTs: a highly active and stable catalyst for the generation of COx-free hydrogen in ammonia decomposition. *Appl. Catal., B* **2004**, *48*, 237−241.

(33) Zhang, J.; Xu, H.; Ge, Q.; Li, W. Highly efficient Ru/MgO catalysts for NH3 decomposition: Synthesis, characterization and promoter effect. *Catal. Commun.* **2006**, *7*, 148−152.

(34) Hayashi, F.; Toda, Y.; Kanie, Y.; Kitano, M.; Inoue, Y.; Yokoyama, T.; Hara, M.; Hosono, H. Ammonia decomposition by ruthenium nanoparticles loaded on inorganic electride C12A7:e. *Chem. Sci.* **2013**, *4*, 3124−3130.

(35) Li, L.; Zhu, Z. H.; Yan, Z. F.; Lu, G. Q.; Rintoul, L. Catalytic ammonia decomposition over Ru/carbon catalysts: The importance of the structure of carbon support. *Appl. Catal., A* **2007**, *320*, 166−172.

(36) Zheng, W.; Zhang, J.; Zhu, B.; Blume, R.; Zhang, Y.; Schlichte, K.; Schlögl, R.; Schüth, F.; Su, D. S. Structure−function correlations for Ru/CNT in the catalytic decomposition of ammonia. *ChemSusChem* **2010**, *3*, 226−230.

(37) Raróg-Pilecka, W.; Miśkiewicz, E.; Szmigiel, D.; Kowalczyk, Z. Structure sensitivity of ammonia synthesis over promoted ruthenium catalysts supported on graphitised carbon. *J. Catal.* **2005**, *231*, 11−19.

(38) Garcia-Garcia, F.; Guerrero-Ruiz, A.; Rodriguez-Ramos, I. Role of B5-type sites in Ru catalysts used for the NH_3 decomposition reaction. *Top. Catal.* **2009**, *52*, 758−764.

(39) Karim, A. M.; Prasad, V.; Mpourmpakis, G.; Lonergan, W. W.; Frenkel, A. I.; Chen, J. G.; Vlachos, D. G. Correlating particle size and shape of supported Ru/γ-Al_2O_3 catalysts with NH_3 decomposition activity. *J. Am. Chem. Soc.* **2009**, *131*, 12230−12239.

(40) Kresse, G.; Furthmuller, J. Efficient iterative schemes for ab initio total-energy calculations using plane wave basis set. *Phys. Rev. B: Condens. Matter Mater. Phys.* **1996**, *54*, 11169−11186.

(41) Kresse, G.; Furthmuller, J. Efficiency of ab initio total energy calculations for metals and semiconductors using plane wave basis set. *Comput. Mater. Sci.* **1996**, *6*, 15−50.

(42) Perdew, J. P.; Burke, K.; Ernzerhof, M. Generalized gradient approximation made simple. *Phys. Rev. Lett.* **1996**, *77*, 3865−3868.

(43) Blöchl, P. E. Projector augmented-wave method. *Phys. Rev. B: Condens. Matter Mater. Phys.* **1994**, *50*, 17953−17979.

(44) Monkhorst, H. J.; Pack, J. D. Special points for Brillouin-zone integrations. *Phys. Rev. B* **1976**, *13*, 5188−5192.

(45) Grimme, S. Semiempirical GGA-type density functional constructed with a long-range dispersion correction. *J. Comput. Chem.* **2006**, *27*, 1787−1799.

(46) Henkelman, G.; Jónsson, H. Improved tangent estimate in the nudged elastic band method for finding minimum energy paths and saddle points. *J. Chem. Phys.* **2000**, *113*, 9978−9985.

(47) Bader, R. F. W. A quantum theory of molecular structure and its applications. *Chem. Rev.* **1991**, *91*, 893−928.

(48) Verdinelli, V.; Germán, E.; Luna, C. R.; Marchetti, J. M.; Volpe, M. A.; Juan, A. Theoretical Study of Hydrogen Adsorption on Ru-Decorated (8,0) Single-Walled Carbon Nanotube. *J. Phys. Chem. C* **2014**, *118*, 27672−27680.

(49) Wang, L. L.; Johnson, D. D. Density functional study of structural trends for late-transition-metal 13-atom clusters. *Phys. Rev. B: Condens. Matter Mater. Phys.* **2007**, *75*, 235405.

(50) Chang, C. M.; Chou, M. Y. Alternative low-symmetry structure for 13-atom metal clusters. *Phys. Rev. Lett.* **2004**, *93*, 133401.

(51) Bae, Y.-C.; Osanai, H.; Kumar, V.; Kawazoe, Y. Atomic structures and magnetic behavior of small ruthenium clusters. *Mater. Trans.* **2005**, *46*, 159−162.

(52) Li, S.; Li, H.; Liu, J.; Xue, X.; Tian, Y.; He, H.; Jia, Y. Structural and electronic properties of Ru_n clusters ($n = 2−14$) studied by first-

principles calculations. *Phys. Rev. B: Condens. Matter Mater. Phys.* **2007**, *76*, 045410.

(53) Chen, H.-Y. T.; Tosoni, S.; Pacchioni, G. Adsorption of ruthenium atoms and clusters on anatase TiO_2 and tetragonal $ZrO_2(101)$ surfaces: a comparative DFT study. *J. Phys. Chem. C* **2015**, *119*, 10856−10868.

(54) Liu, X.; Yao, K. X.; Meng, C. G.; Han, Y. Graphene substrate-mediated catalytic performance enhancement of Ru nanoparticles: a first-principles study. *Dalton Trans.* **2012**, *41*, 1289−1296.

(55) Gao, H.; Zhao, J. First-principles study of Ru atoms and clusters adsorbed outside and inside carbon nanotubes. *J. Chem. Phys.* **2010**, *132*, 234704.

(56) Schwegmann, S.; Seitsonen, A. P.; Dietrich, H.; Bludau, H.; Over, H.; Jacobi, K.; Ertl, G. The adsorption of atomic nitrogen on Ru(0001): geometry and energetics. *Chem. Phys. Lett.* **1997**, *264*, 680−686.

(57) Mortensen, H.; Diekhöner, L.; Baurichter, A.; Jensen, E.; Luntz, A. C. Dynamics of ammonia decomposition on Ru(0001). *J. Chem. Phys.* **2000**, *113*, 6882−6887.

(58) Diekhöner, L.; Baurichter, A.; Mortensen, H.; Luntz, A. C. Observation of metastable atomic nitrogen adsorbed on Ru (0001). *J. Chem. Phys.* **2000**, *112*, 2507−2515.

(59) Mortensen, J. J.; Morikawa, Y.; Hammer, B.; Nørskov, J. K. Density functional calculations of N_2 adsorption and dissociation on a Ru(0001) surface. *J. Catal.* **1997**, *169*, 85−92.

(60) Andzelm, J.; Govind, N.; Maiti, A. Nanotube-based gas sensors − Role of structural defects. *Chem. Phys. Lett.* **2006**, *421*, 58−62.

(61) Molina, L. M.; Hammer, B. Active role of oxide support during CO oxidation at Au/MgO. *Phys. Rev. Lett.* **2003**, *90*, 206102.

(62) Guo, S.; Pan, X.; Gao, H.; Yang, Z.; Zhao, J.; Bao, X. Probing the electronic effect of carbon nanotubes in catalysis: NH_3 synthesis with Ru nanoparticles. *Chem. - Eur. J.* **2010**, *16*, 5379−5384.

(63) Kim, H. Y.; Lee, H. M.; Henkelman, G. CO oxidation mechanism on CeO_2-supported Au nanoparticles. *J. Am. Chem. Soc.* **2012**, *134*, 1560−1570.

(64) Wang, Y.-G.; Yoon, Y.; Glezakou, V.-A.; Li, J.; Rousseau, R. The role of reducible oxide−metal cluster charge transfer in catalytic processes: New insights on the catalytic mechanism of CO oxidation on Au/TiO2 from ab initio molecular dynamics. *J. Am. Chem. Soc.* **2013**, *135*, 10673−10683.

(65) Liu, B.; Liu, J.; Li, T.; Zhao, Z.; Gong, X.-Q.; Chen, Y.; Duan, A.; Jiang, G.; Wei, Y. Interfacial effects of CeO_2-supported Pd nanorod in catalytic CO oxidation: A theoretical study. *J. Phys. Chem. C* **2015**, *119*, 12923−12934.